Proc. R. Soc. Lond. A **406**, 205–226 (1986)
Printed in Great Britain

Bending effects on flow localization in metallic sheets

BY N. TRIANTAFYLLIDIS† AND SHYAM K. SAMANTA‡

† *Aerospace Engineering Department, The University of Michigan, Ann Arbour, Michigan* 48109, *U.S.A.*

‡ *Metallurgy Department Research Staff, Ford Motor Company, Dearborn, Michigan* 48121-2053, *U.S.A.*

(*Communicated by O. C. Zienkiewicz, F.R.S. – Received* 20 *March* 1985 *– Revised* 6 *January* 1986)

[Plate 1]

In the present work the dependence of critical strain on thickness in finitely stretched metallic sheets is investigated. A finite strain axisymmetric shell theory is developed for the modelling of the punch stretching of a thick circular plate and a consistent onset of localization criterion for the shell is proposed.

Experimental results as well as numerical calcutions, in the case of mild steel plates deforming under the action of a frictionless hemispherical punch, show that if the onset of strain localization is used as the failure criterion, the material's thickness has very little influence for plate thicknesses usually used in sheet forming. The opposite held viewpoint in the literature that the sheet thickness significantly affects the critical strain is due to the experimental use of the fracture strain as the failure strain.

1. INTRODUCTION

One of the most important problems arising in sheet metal-forming operations is the determination of ductility limits for biaxially stretched sheets, due to the onset of localized necking. Although many materials can be stretched far beyond the point of initial strain localization till actual failure (usually by fracture), in sheet metal forming localized necking itself is considered to be unacceptable. To this end the widely used concept of the forming limit diagram (Keeler & Backofen 1963), to be henceforth abbreviated by FLD, is meant to furnish the final critical strain of a thin sheet as a function of the ratio, ρ^*, of the principal strains, e_1 and e_2, ($\rho^* = e_1/e_2$) in an e_1–e_2 diagram.

The experimental determination of a particular material's FLD most often consists of stretching a thin sheet of the material in question up to the point of failure, over a rigid hemispherical punch under various frictional constraints in order to achieve different principal critical strain ratios ρ^*.

The list of variables and issues thought to be of importance for the theoretical prediction of a given metal's FLD, based on fundamental mechanical properties of the material, has grown to be confusingly long. The main thrust of the research in this area has been focused on the choice of a proper constitutive law by

including not only strain hardening and plastic anisotropy effects but also strain rate sensitivity, internal damage (in terms of microscopic void nucleation and growth), choice of smooth against vertex type yield surface and so on. Almost invariably, in all theoretical treatments the sheet is idealized as a thin membrane (i.e. bending stiffness is ignored) and plane stress conditions are invoked. In spite of the widely accepted viewpoint of higher formability associated with thicker sheet metals (see, for example, Hecker (1978) and references quoted therein), much less effort has been devoted in investigating the effect of the sheet's thickness on its ductility limits.

One of the earliest experimental investigations in this direction appears to be the work by Kula & Fahen (1961) on tensile testing, although the specimen thicknesses used were beyond the range of interest in sheet metal forming. Of more relevance to our purpose are the most recent experimental works on punch stretching by Hiam & Lee (1978) and by Hecker (1978). The materials used by Hiam & Lee (1978) however had different compositions and furthermore had undergone such variations in manufacturing processing (some specimens were hot rolled while others were cold rolled) that it is impossible to assess the distinction between the thickness and the plastic anisotropy effects. On the other hand, Hecker's (1978) investigations on 1100 aluminium were more complete and conclusive. His experimental results show that there is a distinct advantage of using thicker sheets, in terms of formability as measured by the earlier described conventional technique.

On the theoretical side, the only investigation so far dealing with the effects of thickness on the limiting strains of metallic sheets appears to be the one by Hutchinson *et al.* (1978) on the validity of the plane stress assumption under uniaxial plane strain tension. In this work the growth of small amplitude (in thickness variation) waves with increasing strain was examined and compared for both the one-dimensional plane stress and the exact two-dimensional plane strain calculations using a particular rate sensitive (of the power law type) constitutive equation. So far no similar effort has been made to analyse the problem of punch stretching to investigate the effects of sheet thickness on forming limits of metallic sheets. The express desire of the present investigation is to propose an analytical method of modelling the deformation of a metallic sheet bent over a curved punch and to predict its ductility limit as a function of the sheet's thickness.

The starting point for the analysis is the construction of an appropriate (axisymmetric) finite displacement and finite rotation shell theory capable of accommodating a wide class of rate independent constitutive equations at arbitrary levels of strain. The most interesting feature of the proposed theory (which admits a full Lagrangian formulation) is that it uses the current axial force and bending moment resultants as its stress measures and, due to an appropriate choice of the corresponding strain measures, it always satisfies the exact equilibrium equations at the current configuration. Although a great number of both geometric and material nonlinear shell theories have been devised previously, the shell theory used in this work is novel. For this reason and also for continuity a brief, self-contained presentation of the proposed shell theory has been included in this paper.

The onset of strain localization during the deformation process is indicated in the analysis by a change in character of the governing incremental equilibrium equations at some location, i.e. they become singular. When this occurs, the existence of a zone containing strain rate discontinuities becomes possible and strain starts accumulating selectively in that region when additional overall deformation is imposed. The advantage of this approach is the existence of a closed form localization criterion. It also implies that the usually undesirable and troublesome assumption of a pre-existing initial imperfection in the sheet (the so-called 'Marciniak' (Marciniak & Kuczynski 1967) approach), which is a concept frequently employed in studies of sheet metal ductility, is unnecessary.

For reasons to be elaborated in detail in the next section, all the calculations reported in this work have been performed using a rate independent plasticity law based on a model introduced by Christoffersen & Hutchinson (1979) and whose novelty consists of introducing a smooth dependence of the incremental moduli on the stress or strain rates. The model's parameter that have been directly determined by independent experiments (such as the yield stress, the hardening exponent, the plastic anisotropy ratio and so on) have been kept fixed in all calculations. A finite element discretization of the governing equilibrium equations provided the basis for numerical computations reported here.

The effect of geometry (aperture to punch radius ratio) on the radial critical strain (e_1) against thickness to radius of curvature (h/R_p) curves has been investigated. In addition, the effect of the model's strain rate dependence of the incremental moduli (which have been established indirectly so that the computations match the experimental data for thin sheets) has been explored. It should also be noted here that, because of the absence of friction from the experiments modelled, all results obtained are near the balanced biaxial régime of the FLD.

The experimental investigations were carried out on sheets of mild steel of two different thicknesses, h (0.028 in and 0.056 in†), with the use of hemispherical punches of different radii, R_p, in order to achieve thickness:radius of curvature ratios (h/R_p) ranging from approximately 0.015 to 0.056. Tests were conducted up to the onset of localized necking (in contrast to the usual test procedures in which the specimen is deformed up to fracture) and results have been compared with corresponding numerical calculations. The presentation is concluded by a critical evaluation of the obtained results.

2. Formulation

The general formulation for large displacements and rotations-large strains deformation of a shell of revolution under axisymmetric loading will be presented here. From the principle of virtual work in conjunction with the exact equilibrium equations in the current configuration, one can establish the existence of an appropriate set of (finite) strain measures, work conjugate to the stress measures employed by the theory. For a wide class of rate independent elastic–plastic materials the rates of the aforementioned strain measures also appear in the rate

† 1 in = 2.54 cm.

form of the constitutive equations for the stress measures, which in this theory are the current resultant forces and bending moments of the shell.

2.1. *Equilibrium equations and strain measures*

Let $\mathscr{S}$ denote the reference configuration of the shell's middle surface whose fixed axis of symmetry is OA, where A is the apex of $\mathscr{S}$ (see figure 1*a*). The intersection of $\mathscr{S}$ with a plane passing through OA and forming an angle θ with the Ox axis is the curve $\mathscr{C}$. Moreover $\boldsymbol{t}, \boldsymbol{n}, \boldsymbol{b}$ is an orthonormal triad with $\boldsymbol{t}$ tangent to $\mathscr{C}$ and $\boldsymbol{n}$ the outward normal to $\mathscr{S}$ at a point at a radial distance ρ from the symmetry axis OA. In addition, ϕ denotes the angle between $\boldsymbol{n}$ and OA, s the arch length parameter on $\mathscr{C}$ and $\boldsymbol{r}(s, \theta)$ is the position vector of a material point on $\mathscr{S}$ as shown in figure 1*a*, *b*. The same symbols surmounted by a bar ($\bar{}$) are used for the corresponding quantities in the current configuration.

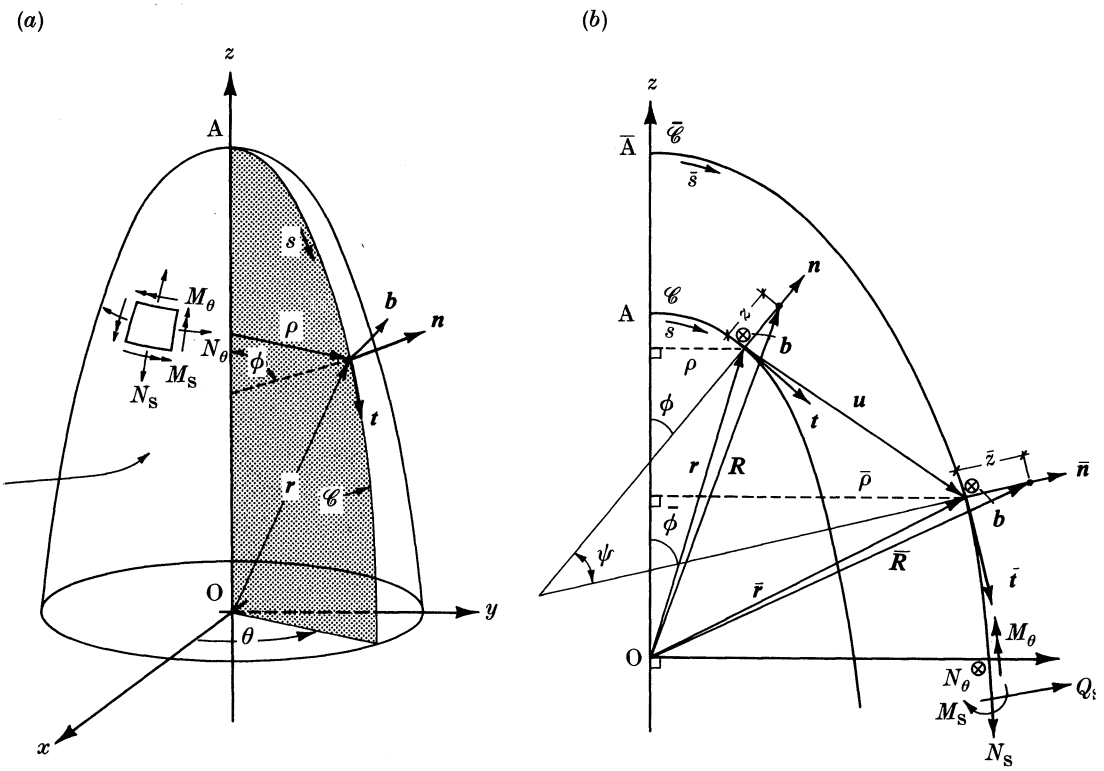

FIGURE 1. (*a*) Undeformed configuration for the axisymmetric shell's reference surface, (*b*) undeformed (and deformed) configuration of the generator curve $\mathscr{C}$ (and $\bar{\mathscr{C}}$) for the axisymmetric shell.

Starting with the kinematics of the problem, the current position $\bar{\boldsymbol{r}}$ of a material point initially at $\boldsymbol{r}$ is given by

$$\bar{\boldsymbol{r}} = \boldsymbol{r} + \boldsymbol{u} = \boldsymbol{r} + v\boldsymbol{t} + w\boldsymbol{n}, \tag{2.1}$$

where $v(s)$ and $w(s)$ are the components of the displacement vector $\boldsymbol{u}$ with respect

to the $\boldsymbol{t}, \boldsymbol{n}, \boldsymbol{b}$ basis. Employing the well-known Frenet formulas (see, for example, Goetz 1970) for the planar curve $\mathscr{C}(\bar{\mathscr{C}})$ namely:

$$\partial \boldsymbol{t}/\partial s = -k_s \boldsymbol{n}, \ (\partial \bar{\boldsymbol{t}}/\partial \bar{s} = -\bar{k}_s \bar{\boldsymbol{n}}); \ \partial \boldsymbol{n}/\partial s = k_s \boldsymbol{t}, \ (\partial \bar{\boldsymbol{n}}/\partial \bar{s} = \bar{k}_s \bar{\boldsymbol{t}}), \tag{2.2}$$

where $k_s(\bar{k}_s)$ is the curvature of $\mathscr{C}(\bar{\mathscr{C}})$ and where the tangent vector $\boldsymbol{t}(\bar{\boldsymbol{t}})$ of $\mathscr{C}(\bar{\mathscr{C}})$ is

$$\boldsymbol{t} = \partial \boldsymbol{r}/\partial s, \quad (\bar{\boldsymbol{t}} = \partial \bar{\boldsymbol{r}}/\partial \bar{s}), \tag{2.3}$$

in conjunction with (2.1), the principal stretch ratio, λ_s, in the tangential direction of the shell along $\mathscr{C}$ is found to be

$$\lambda_s = \mathrm{d}\bar{s}/\mathrm{d}s = [(1+e)^2+f^2]^{\frac{1}{2}}, \tag{2.4}$$

in which e and f are defined by

$$e \equiv \mathrm{d}v/\mathrm{d}s + k_s w, \quad f \equiv \mathrm{d}w/\mathrm{d}s - k_s v. \tag{2.5}$$

The other principal stretch ratio, λ_θ, in a direction perpendicular to $\mathscr{C}$ is

$$\lambda_\theta = \bar{\rho}/\rho. \tag{2.6}$$

From (2.1)–(2.5) one can obtain for the current tangent and normal to $\bar{\mathscr{C}}$

$$\bar{\boldsymbol{t}} = (1+e)/\lambda_s \boldsymbol{t} + f/\lambda_s \boldsymbol{n}, \quad \bar{\boldsymbol{n}} = -(f/\lambda_s)\boldsymbol{t} + (1+e)/\lambda_s \boldsymbol{n} \tag{2.7}$$

from which it can be easily deduced that the angle ψ formed between $\bar{\boldsymbol{t}}$ and $\boldsymbol{t}$ (or the same between $\bar{\boldsymbol{n}}$ and $\boldsymbol{n}$) satisfies

$$\cos\psi = (1+e)/\lambda_s, \quad \sin\psi = -f/\lambda_s; \quad \psi \equiv \bar{\phi} - \phi. \tag{2.8}$$

From (2.2) and (2.7) one finds the following relationship between the reference (k_s) and current ($\bar{k}_s$) principal curvatures of $\mathscr{S}$ and $\bar{\mathscr{S}}$ along the $\mathscr{C}$ and $\bar{\mathscr{C}}$ directions respectively

$$\lambda_s \bar{k}_s - k_s = [f(\mathrm{d}e/\mathrm{d}s) - (1+e)\,\mathrm{d}f/\mathrm{d}s]/\lambda_s^2. \tag{2.9}$$

The other principal curvatures in the reference (k_θ) and current ($\bar{k}_\theta$) configuration are given by (see, for example, Krauss 1967)

$$k_\theta = (\sin\phi)/\rho, \quad (\bar{k}_\theta = (\sin\bar{\phi})/\bar{\rho}). \tag{2.10}$$

Finally, the following kinematical relationship (obtained from simple geometrical considerations) is recorded at this point for future reference, namely

$$\cos\phi = \mathrm{d}\rho/\mathrm{d}s, \quad (\cos\bar{\phi} = \mathrm{d}\bar{\rho}/\mathrm{d}\bar{s}). \tag{2.11}$$

Assume that N_s and N_θ are the current axial force resultants oriented along $\bar{\boldsymbol{t}}$ and $\bar{\boldsymbol{b}}$ respectively, M_s and M_θ are the current bending moment resultants along $\bar{\boldsymbol{b}}$ and $\bar{\boldsymbol{t}}$ and Q_s is the shear force resultant along $\bar{\boldsymbol{n}}$. The equilibrium equations for $\bar{\mathscr{S}}$ under the influence of distributed loads $\bar{p}_t$ and $\bar{p}_n$ (along $\bar{\boldsymbol{t}}$ and $\bar{\boldsymbol{n}}$) per unit current area, are (see, for example, Krauss 1967)

$$\left.\begin{aligned} (\mathrm{d}/\mathrm{d}\bar{s})(\bar{\rho}N_s) - N_\theta \cos\bar{\phi} + \bar{k}_s(\bar{\rho}Q_s) + \bar{\rho}\bar{p}_t = 0, \\ (\mathrm{d}/\mathrm{d}\bar{s})(\bar{\rho}Q_s) - \bar{k}_s(\bar{\rho}N_s) - N_\theta \sin\bar{\phi} + \bar{\rho}\bar{p}_n = 0, \\ (\mathrm{d}/\mathrm{d}\bar{s})(\bar{\rho}M_s) - M_\theta \cos\bar{\phi} - (\bar{\rho}Q_s) = 0. \end{aligned}\right\} \tag{2.12}$$

The expression for the external virtual work per unit angle, θ, is postulated to be

$$EVW = (\bar{\rho}M_s)\,\delta\chi\Big|_{s_1}^{s_2} + \bar{\rho}Q_s(\delta\boldsymbol{u}\cdot\bar{\boldsymbol{n}})\Big|_{s_1}^{s_2} + \bar{\rho}N_s(\delta\boldsymbol{u}\cdot\bar{\boldsymbol{t}})\Big|_{s_1}^{s_2} + \int_{s_1}^{s_2}[\bar{p}_t(\delta\boldsymbol{u}\cdot\bar{\boldsymbol{t}}) + \bar{p}_n(\delta\boldsymbol{u}\cdot\bar{\boldsymbol{n}})]\,\bar{\rho}\lambda_s\,\mathrm{d}s, \quad (2.13)$$

where χ designates the rotation of the cross section of $\mathscr{S}$ initially perpendicular to $\boldsymbol{t}$. Denoting the work conjugate quantities (linear in δv, δw and $\delta\chi$) of $\lambda_\theta N_s$, $\lambda_s N_\theta$, $\lambda_\theta Q_s$, $\lambda_\theta M_s$ and $\lambda_s M_\theta$ by ϵ_s^*, ϵ_θ^*, γ_s^*, $\hat{k}_s^*$ *and* $\hat{k}_\theta^*$, respectively, the postulated expression for the internal virtual work per unit angle, θ, is

$$IVW = \int_{s_1}^{s_2}[(\lambda_\theta N_s)\,\epsilon_s^* + (\lambda_s N_\theta)\,\epsilon_\theta^* + (\lambda_\theta Q_s)\,\gamma_s^* + (\lambda_\theta M_s)\,\hat{k}_s^* + (\lambda_s M_\theta)\,\hat{k}_\theta^*]\,\rho\,\mathrm{d}s, \quad (2.14)$$

where $s = s_1, s = s_2$ are the two boundaries of $\mathscr{S}$. By equating the external and internal virtual work terms and by using (2.12) as well as the kinematical relations (2.1)–(2.11) the following expression is obtained:

$$\int_{s_1}^{s_2}\{(\lambda_\theta N_s)\,(\epsilon_s^* - \delta\lambda_s) + (\lambda_s N_\theta)\,(\epsilon_\theta^* - \delta\lambda_\theta) + (\lambda_\theta Q_s)\,[\gamma_s^* - \lambda_s\,\delta(\chi - \psi)] + (\lambda_\theta M_s)\,[\hat{k}_s^* - \delta(\mathrm{d}\chi/\mathrm{d}s)] + (\lambda_s M_\theta)\,[\hat{k}_\theta^* - (\cos\bar{\phi})/\rho\,\delta\chi]\}\,\rho\,\mathrm{d}s = 0. \quad (2.15)$$

Assuming that Q_s is a workless reaction force, i.e. $\gamma_s^* = 0$ it follows from (2.15) and the arbitrariness of the values of the stress measures that their work conjugate quantities are exact variations

$$\epsilon_s^* = \delta(\lambda_s), \epsilon_\theta^* = \delta(\lambda_\theta), \hat{k}_s^* = \delta(\mathrm{d}\psi/\mathrm{d}s) = \delta(\lambda_s\bar{k}_s), \hat{k}_\theta^* = \delta[(\sin\bar{\phi})/\rho] = \delta(\lambda_\theta\bar{k}_\theta). \quad (2.16)$$

Hence the finite strain measures ϵ_s, ϵ_θ, $\hat{k}_s$, and $\hat{k}_\theta$ work conjugate to $\lambda_\theta N_s$, $\lambda_s N_\theta$, $\lambda_\theta M_s$ and $\lambda_s M_\theta$ respectively arise in the theory

$$\epsilon_s = \lambda_s - 1, \quad \epsilon_\theta = \lambda_\theta - 1, \quad \hat{k}_s = \lambda_s\bar{k}_s - k_s, \quad \hat{k}_\theta = \lambda_\theta\bar{k}_\theta - k_\theta. \quad (2.17)$$

Note that in the above derivations no assumption has been made about the magnitude of the displacements, the rotations or the strains. In the light of (2.16), the internal virtual work of the shell expressed in the refeence configuration (total Lagrangian description) assumes the form

$$IVW = \int_{s_1}^{s_2}[(\lambda_\theta N_s)\,\delta\epsilon_s + (\lambda_s N_\theta)\,\delta\epsilon_\theta + (\lambda_\theta M_s)\,\delta\hat{k}_s + (\lambda_s M_\theta)\,\delta\hat{k}_\theta]\,\rho\,\mathrm{d}s. \quad (2.18)$$

When the deformation of the shell is due to the advance of an axisymmetric punch in frictionless contact with the shell, as in the process of interest here, the external virtual work term can be written as

$$EVW = -\delta\left[\tfrac{1}{2}k\int_{s_1}^{s_2} d^2H(d)\,\rho\,\mathrm{d}s\right], \quad (2.19)$$

where $d(s)$ is the distance of a point with material coordinate s from the undeformed surface of the punch, (signed positive if the point in question is inside

the punch), $H(x)$ is the Heaviside step function ($H(x) = 0$ for $x < 0$, $H(x) = 1$ for $x \geqslant 0$) and k is an adequately high positive constant. For the specific problem examined in this work, where a hemispherical punch of radius R_p by advancing a vertical distance H penetrates an initially flat circular plate of radius R_A, the distance d takes the form

$$d = R_p - [(\rho + v)^2 + (w + R_p - H)^2]^{\frac{1}{2}}. \tag{2.20}$$

The assumption adopted for the external virtual work term corresponds to a Winkler type foundation for the punch surface where the normal force per unit (reference) area is linearly proportional to the penetration depth, d, with coefficient of proportionality k. For adequately high values of the 'foundation constant', k, the punch surface behaves almost rigidly. Apart from its realistic physical interpretation (in reality no contact can ever be perfectly rigid because there is always a small amount of elastic deformation involved) the advantage of this formulation, usually called a penalty type of formulation in the literature (see, for example, Oden & Kikuchi 1984 and references quoted therein) is that it simplifies considerably the resulting numerical algorithm. Since the method decides automatically which part is in contact with the rigid surface, it avoids complicated iteration schemes, which are usually used in similar analyses of sheet metal forming processes (see, for example, Wang & Budiansky 1978).

The weak formulation of the equilibrium equations is obtained by equating the internal and external virtual work terms (2.18) and (2.19), (2.20), respectively,

$$IVW = EVW \tag{2.21}$$

and it constitutes the basis for the subsequent numerical analysis of the problem.

2.2. *Relations between stress and strain measures for the shell*

Consider a shell of revolution deforming under the action of axisymmetric loads and let $\mathscr{S}$ be the reference surface of the undeformed shell. If $\boldsymbol{R}$ is the position vector of a material point M in the reference configuration, then

$$\boldsymbol{R}(s, \theta, z) = \boldsymbol{r}(s, \theta) + z\boldsymbol{n}(s, \theta), h_1(s) \leqslant z \leqslant h_2(s), \quad (h_1 = -\tfrac{1}{2}h, h_2 = \tfrac{1}{2}h), \tag{2.22}$$

where z is the distance of the material point in question from $\mathscr{S}$, h is the initial plate thickness, and $\boldsymbol{r}$ is the position vector of the foot of the normal from M to $\mathscr{S}$. For the current configuration the normality assumption, i.e. cross sections normal to $\mathscr{S}$ remain normal to $\bar{\mathscr{S}}$, is adopted in agreement with the kinematical hypothesis $\gamma_s^* = 0$ (no transverse shear deformation) made in the previous subsection. The current position vector $\bar{\boldsymbol{R}}$ of material point M, initially at $\boldsymbol{R}$, is thus given by

$$\bar{\boldsymbol{R}}(s, \theta, z) = \bar{\boldsymbol{r}}(s, \theta) + \bar{z}(s, z)\,\bar{\boldsymbol{n}}(s, \theta), \tag{2.23}$$

with $\bar{z}$ the current distance of the material M point from $\bar{\mathscr{S}}$.

A full Lagrangian formulation of the problem is adopted (in conformity to the analysis in the previous subsection) with convected coordinates $s = \theta^1, \theta = \theta^2$,

$z = \theta^3$. Consequently, the covariant components of the undeformed metric tensor G_{ij}† are found to be

$$G_{ij} = (\partial \boldsymbol{R}/\partial\theta^i)\cdot(\partial \boldsymbol{R}/\partial\theta^j); \quad G_{11} = (1+k_s z)^2, \quad G_{22} = [\rho(1+k_\theta z)]^2,$$
$$G_{33} = 1, \quad G_{ij} = 0 \quad \text{for} \quad i \neq j \qquad (2.24)$$

whereas the corresponding components of the current metric tensor $\bar{G}_{ij}$ are

$$\bar{G}_{ij} = (\partial \bar{\boldsymbol{R}}/\partial\theta^i)\cdot\partial \bar{\boldsymbol{R}}/\partial\theta^j); \quad \bar{G}_{11} = [\lambda_s(1+\bar{k}_s \bar{z})]^2, \quad \bar{G}_{22} = [\bar{\rho}(1+\bar{k}_\theta \bar{z})]^2,$$
$$\bar{G}_{33} = (\partial\bar{z}/\partial z)^2, \quad \bar{G}_{ij} = 0 \quad \text{if} \quad i \neq j \qquad (2.25)‡$$

when the thickness variation $\partial\bar{z}/\partial s$ term is considered negligible.

The notion of the rate of a field quantity is introduced at this point and it is defined to be the derivative of the quantity in question with respect to some monotonically increasing parameter characterizing the deformation history; it is denoted by a dot ($\dot{}$) on top of the symbol of the variable in question. For a fairly broad class of materials which incorporates as special cases hyperelastic, hypoelastic as well as rate independent elastoplastic ones the (three-dimensional) material constitutive equation can be put in the form

$$\dot{\tau}^{ij} = L^{ijkl}\dot{E}_{kl}; \quad \dot{E}_{kl} = \tfrac{1}{2}\dot{\bar{G}}_{kl}, \qquad (2.26)$$

where $\dot{\tau}^{ij}$ are the contravariant components of the Kirchhoff stress, $\dot{E}_{ij}$ the covariant components of the strain rate and L^{ijkl} are the contravariant components of the incremental moduli tensor $\boldsymbol{L}$, all with respect to the current basis. The tensor $\boldsymbol{L}$ may in general depend on the current metric, current stress state, material properties as well as the 'loading direction' in stress (or strain) space as will be specified later. The incremental moduli tensor will be endowed with the symmetry $L^{ijkl} = L^{klij}$ (in addition to the trivial ones $L^{ijkl} = L^{jikl} = L^{jilk}$).

By assuming that every point of the shell is at a state of approximately plane stress, i.e. $\tau^{3i} = \dot{\tau}^{3i} = 0$ and by using the axisymmetrical implication $\tau^{12} = \dot{\tau}^{12} = \dot{E}_{12} = 0$ one deduces from (2.26) that

$$\dot{\tau}^{11} = \frac{\mathscr{L}^{\langle 11\rangle}}{\bar{G}_{11}\bar{G}_{11}}\dot{E}_{11} + \frac{\mathscr{L}^{\langle 12\rangle}}{\bar{G}_{11}\bar{G}_{22}}\dot{E}_{22}, \quad \dot{\tau}^{22} = \frac{\mathscr{L}^{\langle 21\rangle}}{\bar{G}_{22}\bar{G}_{11}}\dot{E}_{11} + \frac{\mathscr{L}^{\langle 22\rangle}}{\bar{G}_{22}\bar{G}_{22}}\dot{E}_{22} \qquad (2.27)$$

with the physical components of the plane stress moduli $\mathscr{L}^{\langle\alpha\beta\rangle}$ given in terms of the physical components $L^{\langle ijkl\rangle}$ of $\boldsymbol{L}$ by

$$\mathscr{L}^{\langle\alpha\beta\rangle} = L^{\langle\alpha\alpha\beta\beta\rangle} - L^{\langle\alpha\alpha 33\rangle}L^{\langle 33\beta\beta\rangle}/L^{\langle 3333\rangle} \quad \alpha,\beta = 1,2 \text{ (no sum)}. \qquad (2.28)$$

Expressing the stress measures for the shell, introduced in the previous subsection, as thickness integrals of the appropriate Cauchy stress components it is found that:

† Here and subsequently Latin indices range from 1 to 3.

‡ In the derivation of (2.24) and (2.25) use was made of the relations $\partial\boldsymbol{r}/\partial\theta = \rho\boldsymbol{b}$, $(\partial\bar{\boldsymbol{r}}/\partial\theta = \bar{\rho}\bar{\boldsymbol{b}})$ and $\partial\boldsymbol{n}/\partial\theta = \sin\phi\boldsymbol{b}(\partial\bar{\boldsymbol{n}}/\partial\theta = \sin\bar{\phi}\bar{\boldsymbol{b}})$.

$$\left.\begin{aligned}
\lambda_\theta N_s &= \frac{\bar\rho}{\rho}\int_{h_1}^{h_2}\sigma^{\langle 11\rangle}(1+\bar k_\theta\bar z)\frac{\partial\bar z}{\partial z}\,\mathrm{d}z, \quad \lambda_s N_\theta = \lambda_s\int_{h_1}^{h_2}\sigma^{\langle 22\rangle}(1+\bar k_s\bar z)\frac{\partial\bar z}{\partial z}\,\mathrm{d}z,\\
\lambda_\theta M_s &= \frac{\bar\rho}{\rho}\int_{h_1}^{h_2}\sigma^{\langle 11\rangle}(1+\bar k_\theta\bar z)\,\bar z\frac{\partial\bar z}{\partial z}\,\mathrm{d}z, \quad \lambda_s M_\theta = \lambda_s\int_{h_1}^{h_2}\sigma^{\langle 22\rangle}(1+\bar k_s\bar z)\,\bar z\frac{\partial\bar z}{\partial z}\,\mathrm{d}z
\end{aligned}\right\} \tag{2.29}$$

which with the help of (2.27), (2.28) and(2.24)–(2.26) and recalling that

$$\tau^{ij} = \sigma^{ij}(\det\bar G_{ij}/\det G_{ij})^{\frac{1}{2}}$$

lead to the following expressions relating the rates of the stress measures to those of the strain measures:

$$\left.\begin{aligned}
(\lambda_\theta N_s)^{\cdot} &= C^{11}_{11}\dot\epsilon_s + C^{12}_{11}\dot\epsilon_\theta + C^{11}_{12}\dot{\bar k}_s + C^{12}_{12}\dot{\bar k}_\theta,\\
(\lambda_s N_\theta)^{\cdot} &= C^{12}_{11}\dot\epsilon_s + C^{22}_{11}\dot\epsilon_\theta + C^{12}_{12}\dot{\bar k}_s + C^{22}_{12}\dot{\bar k}_\theta,\\
(\lambda_\theta M_s)^{\cdot} &= C^{11}_{12}\dot\epsilon_s + C^{12}_{12}\dot\epsilon_\theta + C^{11}_{22}\dot{\bar k}_s + C^{12}_{22}\dot{\bar k}_\theta,\\
(\lambda_s M_\theta)^{\cdot} &= C^{12}_{12}\dot\epsilon_s + C^{22}_{12}\dot\epsilon_\theta + C^{12}_{22}\dot{\bar k}_s + C^{22}_{22}\dot{\bar k}_\theta,
\end{aligned}\right\} \tag{2.30}$$

where the coefficients $C^{\alpha\beta}_{\gamma\delta}$ are given by

$$\left.\begin{aligned}
C^{\alpha\beta}_{\gamma\delta} &= \int_{h_1}^{h_2}\frac{\mathscr{L}^{\langle\alpha\beta\rangle}+\tau^{\langle\alpha\beta\rangle}}{\bar H_\alpha\bar H_\beta}(\bar z)^{\gamma+\delta-2}(1+k_s z)(1+k_\theta z)\,\mathrm{d}z \text{ (no sum) } \alpha,\beta,\gamma,\delta = 1,2.\\
\bar H_1 &\equiv \lambda_s(1+\bar k_s\bar z), \quad \bar H_2 \equiv \lambda_\theta(1+\bar k_\theta\bar z).
\end{aligned}\right\} \tag{2.31}$$

Note that in the (independently derived, based on three-dimensional considerations) rate form of the stress-measure–strain-measure relation for the proposed shell theory, the strain measures found in the previous subsection reappear in a natural way.

2.3. *Localization criterion*

The localization criterion to be adopted for the finitely strained axisymmetric shell is the onset of a discontinuous solution in the form of an annular zone, which conforms with experimental observations in the axisymmetric punch test. The corresponding analytical model requires the investigation of singular points in the incremental equilibrium equations governing the deformation of the shell. The analysis here is the same in spirit with the work of Hill (1952) for the plane stress localization problem, the main difference being that the corresponding differential equations in this case are of higher order in terms of the displacement variables.

The starting point for the localization analysis is the following form of the equilibrium equations of the shell, derivable from (2.12) and expressed with respect to the reference configuration.

$$\left.\begin{aligned}
&(\mathrm{d}/\mathrm{d}s)(\rho\lambda_\theta N_s) - (\lambda_s N_\theta)\cos\bar\phi + \bar k_s(\mathrm{d}/\mathrm{d}s)(\rho\lambda_\theta M_s)\\
&\qquad - \bar k_s\cos\bar\phi(\lambda_s M_\theta) + \bar\rho\lambda_s\bar p_t = 0,\\
&(\mathrm{d}/\mathrm{d}s)[(1/\lambda_s)(\mathrm{d}/\mathrm{d}s)(\rho\lambda_\theta M_s)] - (\mathrm{d}/\mathrm{d}s)[\cos\bar\phi(\lambda_s M_\theta)/\lambda_s]\\
&\qquad - \bar k_s\lambda_s\rho(\lambda_\theta N_s) - \sin\bar\phi(\lambda_s N_\theta) + \bar\rho\lambda_s\bar p_n = 0.
\end{aligned}\right\} \tag{2.32}$$

Taking the rate form of (2.32) in combination with (2.30) and subsequently identifying the reference configuration with the current one, so that $v = w = 0$ but $\dot{v}, \dot{w} \neq 0$ (updated Lagrangian approach), one obtains the following system of differential equations linear in $\dot{v}, \dot{w}$ and their derivatives with respect to $\bar{s}$.

$$(\bar{C}^{11}_{11} + \bar{k}_s \bar{C}^{11}_{12})(\mathrm{d}^2\dot{v}/\mathrm{d}\bar{s}^2) + (\bar{C}^{11}_{12} + \bar{k}_s \bar{C}^{11}_{22})(-\mathrm{d}^3\dot{w}/\mathrm{d}\bar{s}^3 + \bar{k}_s \mathrm{d}^2\dot{v}/\mathrm{d}\bar{s}^2)\,\bar{C}^{11}_{12}(\mathrm{d}^3\dot{v}/\mathrm{d}\bar{s}^3) + \bar{C}^{11}_{22}(-\mathrm{d}^4\dot{w}/\mathrm{d}\bar{s}^4 + \bar{k}\,\mathrm{d}^3\dot{v}/\mathrm{d}\bar{s}^3) + \text{LOT} = 0, \quad (2.33)\dagger$$

where LOT designates the lower order derivatives of $\dot{v}, \dot{w}$. Assuming that at a given state of deformation a discontinuous solution for $\dot{v}, \dot{w}$ becomes possible across the line $\bar{s} = \bar{s}^*$ and denoting by $\Delta(\ )$ the jump of any field quantity across the aforementioned line of discontinuity, one obtains from (2.33)

$$\left.\begin{aligned}(\bar{C}^{11}_{11} + \bar{k}_s \bar{C}^{11}_{12})\,\Delta(\mathrm{d}^3\dot{v}/\mathrm{d}\bar{s}^3) + (\bar{C}^{11}_{12} + \bar{k}_s \bar{C}^{11}_{22})\,\Delta(-\mathrm{d}^4\dot{w}/\mathrm{d}\bar{s}^4 + \bar{k}_s \mathrm{d}^3\dot{v}/\mathrm{d}\bar{s}^3) = 0,\\ \bar{C}^{11}_{12}\,\Delta(\mathrm{d}^3\dot{v}/\mathrm{d}\bar{s}^3) + \bar{C}^{11}_{22}\,\Delta(-\mathrm{d}^4\dot{w}/\mathrm{d}\bar{s}^4 + \bar{k}_s \mathrm{d}^3\dot{v}/\mathrm{d}\bar{s}^3) = 0.\end{aligned}\right\} \quad (2.34)$$

Here the discontinuity is assumed only in the highest order derivatives of the tangent $\dot{v}$ and normal $\dot{w}$ displacement increments. A non-trivial solution to (2.34) becomes possible if

$$\bar{C}^{11}_{11}\bar{C}^{11}_{22} - (\bar{C}^{11}_{12})^2 = 0. \quad (2.35)$$

For as long as the left-hand side of the above equation is positive no localization instability occurs. The first time (as the punch depth, H, increases) that the above criterion is met for a given $\bar{s} = \bar{s}^*$ (i.e. the first time that the incremental equilibrium equations for the shell admit a singular point), localization failure is considered to have occurred.

It is not difficult to show that for the limiting case as $h \to 0\,(h_1, h_2 \to 0)$ one recovers the localization criterion for membranes under biaxial tension, i.e. $\mathscr{L}^{\langle 11\rangle} + \tau^{\langle 11\rangle} = 0$ (see Stören & Rice 1975). In addition, if $\mathscr{L}^{\langle 11\rangle} + \tau^{\langle 11\rangle} > 0$ consistently during the past deformation history for every point $(\bar{s}, \bar{z})$ in the shell (i.e. $\bar{s}_1 \leqslant \bar{s} \leqslant \bar{s}_2, h_1 \leqslant \bar{z} \leqslant h_2$) the determinant in (2.35) is always positive and thus stability against localization is implied up to the current state. A general version of the above localization criterion for doubly curved shells is given by Triantafyllidis (1985*b*).

2.4. *Constitutive model adopted for the material investigated*

In Hill's (1952) well-known analysis for the onset of localized necking of thin flat metallic sheets, based on the classical smooth yield surface rigid plasticity theory, no necking is predicted under biaxial stretching conditions. The incorporation of the elastic part of the strain in the constitutive equations makes very little difference in the localization predictions which in this case are found to give unrealistically high levels of stress at necking (of the order of the elastic moduli). In order to account for localized necking under biaxial stretching conditions, two

† $\bar{C}^{\alpha\beta}_{\gamma\delta}$ are the coefficients in (2.31) evaluated for a shell with coinciding current and reference configurations.

different approaches have been proposed. One, initiated by Marciniak & Kuczynski 1967, postulates the existence of an initial inhomogeneity in the form of a zone appropriately oriented along the final necking direction. This zone is assumed to have different thickness (as for example in Marciniak & Kuczynski 1967) or more generally different material properties than the rest of the sheet as discussed by Needleman & Triantafyllidis (1978). The other method which will be adopted here, in view of its avoidance of the somewhat unrealistic assumption of the favourably oriented weak zone, was proposed by Stören & Rice (1975). In order to model the destabilizing effect of a vertex formed at the current loading point of the yield surface, they used a finite strain version of a simple deformation theory of plasticity, and predicted strain localization under biaxial strain conditions at very realistic strain levels.

The choice of the term 'vertex type' for the class of constitutive equations adopted here is rather unfortunate. What is of importance in the plastic instability analysis is the model's capability to predict reduced, as compared to classical plasticity theories based on an isotropic hardening-smooth yield surface assumption, incremental moduli during abrupt changes from proportional loading. The simplest class of constitutive models found to satisfy this requirement were deformation type theories of plasticity. Because one way of interpreting a deformation theory model within the classical plasticity framework is by appealing to a yield surface with a corner at the current loading point (see, for example, Budiansky 1959) all models with the aforementioned property are usually referred to as 'vertex type' models (in contrast to the 'flow type' ones based on a smooth yield surface and associated flow rule assumption).

The usefulness of the vertex type models for the bifurcation of solids in the plastic range has long been appreciated and deformation type theories of plasticity have successfully and repeatedly been used in the past for plastic buckling calculations (see, for example, Hutchinson (1974) for a comprehensive discussion on the subject). Calculations on rate independent physical theories of metal plasticity, using the single crystal slip model do predict the existence of corners at the current loading point on the yield surface of metal polycrystals (see, for example, Hill 1967; Hutchinson 1970; Lin 1971). Recently, more sophisticated micromechanics calculations on metal polycrystals based on rate sensitive models of slip, do predict the presence of a sharp curvature region at the current loading point of the yield surface (Asaro & Needleman 1984, 1985) rendering plausible the assumption of reduced incremental moduli for increased deviations from proportional loading. Unfortunately, the available experimental evidence is inconclusive (the interested reader is referred to the review article by Hecker 1976), although for certain yield surface definitions a higher curvature at the current loading point seems to appear consistently.

One of the limitations of a simpler deformation type theory of plasticity (as a model for realistic elastic-plastic material) is their validity for nearly proportional loading histories (see, for example, Budiansky 1959). To remedy this situation, Christoffersen & Hutchinson (1979) developed an analytically tractable and more elaborate hybrid between a deformation and a flow type theory of plasticity which has the additional capability of accommodating a smooth dependence of the

incremental moduli tensor on the strain rates, thus mimicking similar features of the more sophisticated physical theories of plasticity mentioned above. A version of their theory, appropriately modified for large strains and which also incorporates transverse plastic anisotropy of the plate, will be used in the subsequent calculations.

Although a detailed presentation of the aforementioned model has been given elsewhere (Triantafyllidis 1985*a*) a brief description is outlined here for completeness.

In this 'corner' theory the instantaneous moduli for nearly proportional loading will be chosen as the moduli of a deformation theory of plasticity (of the isotropic hardening type) and for increased deviation from proportional loading the moduli stiffen monotonically until they coincide with the linearly elastic ones for stress rates directed along or within the corner of the yield surface. For the deformation theory in question (Triantafyllidis 1985*a*) the plastic compliance tensor $\boldsymbol{C}$ is found to be

$$C_{ijkl} = \left(\frac{1}{E_s} - \frac{1}{E}\right)\frac{\partial^2\phi}{\partial\tau^{ij}\,\partial\tau^{kl}} + \frac{1}{\tau_e^2}\left(\frac{1}{E_t} - \frac{1}{E_s}\right)\frac{\partial\phi}{\partial\tau^{ij}}\frac{\partial\phi}{\partial\tau^{kl}}, \tag{2.36}$$†

where τ_e is the equivalent stress for the material given by

$$\tau_e^2 = 2\phi = \frac{(\tau^{\langle 11\rangle} - \tau^{\langle 33\rangle})^2 + (\tau^{\langle 22\rangle} - \tau^{\langle 33\rangle})^2 + R(\tau^{\langle 11\rangle} - \tau^{\langle 22\rangle})^2 + 2(1+2R)\,(\tau^{\langle 12\rangle})^2}{1+R} \tag{2.37}$$

in the case of a transversely plastically anisotropic material with anisotropy ratio R, under plane stress conditions.

The uniaxial behaviour of the material is taken to be a piecewise power law, in which case the secant and tangent moduli E_s and E_t used in (2.36) are

$$E_s = E(\tau_e/\sigma_y)^m, \quad E_t = E_s/m \text{ for } \sigma_y \leqslant \tau_e; \quad E_s = E_t = E \text{ for } \sigma_y > \tau_e, \tag{2.38}$$

where E is Young's modulus of the material, m the hardening exponent and σ_y the yield stress of the uniaxial stress-strain curve. The forward loading cone axis in the stress rate space is taken to be

$$\lambda^{ij} = \tau^{ij}(\tau^{mn}\,C_{mnrs}\,\tau^{rs})^{-\frac{1}{2}} \tag{2.39}$$

and the angular measure, θ, of the deviation of the stress rate direction relative to the above introduced axis is defined by

$$\cos\theta = \lambda^{ij}\,C_{ijkl}\,\overset{\nabla}{\tau}{}^{kl}(\overset{\nabla}{\tau}{}^{mn}\,C_{mnrs}\,\overset{\nabla}{\tau}{}^{rs})^{-\frac{1}{2}}, \tag{2.40}$$‡

where $\overset{\nabla}{\tau}$ is the Jaumann rate of the Kirchhoff stress. The stress rate potential W at the vertex is thus assumed to be

$$W = \tfrac{1}{2}\overset{\nabla}{\tau}{}^{ij}(M_{ijkl} + f(\theta)\,C_{ijkl})\,\overset{\nabla}{\tau}{}^{kl}, \tag{2.41}$$

† The constitutive equations employed here are formulated in terms of the Kirchhoff instead of the Cauchy stresses in view of the resulting symmetries in the incremental moduli discussed in subsection 2.2. The difference between the two stress measures due to elastic compressibility is negligible in plasticity problems.

‡ The angular measure θ of the deviation from proportional loading is not to be confused with the θ coordinate of the axisymmetric shell used in previous subsections.

where $\boldsymbol{M}$ is the well-known tensor of linear elastic compliances with covariant components

$$M_{ijkl} = (1+\nu)/E\,[\tfrac{1}{2}(\bar{G}_{ik}\,\bar{G}_{jl}+\bar{G}_{il}\,\bar{G}_{jk})-\nu/(1+\nu)\,\bar{G}_{ij}\,\bar{G}_{kl}] \tag{2.42}$$

in which ν is the Poisson ratio of the material. The 'transition' function $f(\theta)$ is taken to be

$$f(\theta) = \begin{cases} 1 & \text{for } 0 \leqslant \theta \leqslant \theta_0 \\ \cos^2[\tfrac{1}{2}\pi(\theta-\theta_0)/(\theta_c-\theta_0)] & \text{for } \theta_0 \leqslant \theta < \theta_c \\ 0 & \text{for } \theta_c \leqslant \theta \leqslant \pi \end{cases} \quad (\theta_c-\theta_0 \geqslant \tfrac{1}{2}\pi). \tag{2.43}$$

Finally, the relation between the stress rate and the strain rate assumes the form (in view of the homogeneity of degree two of W in $\overset{\nabla}{\boldsymbol{\tau}}$)

$$\dot{E}_{ij} = \frac{\partial W}{\partial \overset{\nabla}{\tau}_{ij}} = \frac{\partial^2 W}{\partial \overset{\nabla}{\tau}_{ij}\,\partial \overset{\nabla}{\tau}_{kl}}\overset{\nabla}{\tau}_{kl} \Leftrightarrow \overset{\nabla}{\tau}_{ij} = \left(\frac{\partial^2 W}{\partial \overset{\nabla}{\tau}_{ij}\,\partial \overset{\nabla}{\tau}_{kl}}\right)^{-1}\dot{E}_{kl} = L^{ijkl}\,\dot{E}_{kl}, \tag{2.44}$$

with the incremental moduli tensor $\boldsymbol{L}$ (as defined in (2.26)) being the inverse of the compliance tensor $\partial^2 W/\partial\overset{\nabla}{\boldsymbol{\tau}}\,\partial\overset{\nabla}{\boldsymbol{\tau}}$. One can show (see Christoffersen & Hutchinson 1979) that the aforementioned inversion is possible in view of the convexity of W (due to certain properties embodied in $f(\theta)$).

Formulae for the compliance tensor $\partial^2 W/\partial\overset{\nabla}{\boldsymbol{\tau}}\,\partial\overset{\nabla}{\boldsymbol{\tau}}$ as well as some additional details about the proper choice of the yield surface cone angle θ_c will be given in the Appendix.

3. Numerical method

The finite element method is employed in order to solve the boundary value problem discussed in the previous section, i.e. the deformation of a clamped, initially flat circular plate of thickness h due to the advancement by a distance H of a hemispherical punch of radius R_p. The basis for the solution algorithm is the incremental virtual work formulation derived from (2.21) (see also (2.18)–(2.20)) namely,

$$(IVW)^{\cdot} - (EVW)^{\cdot} = -(IVW - EVW). \tag{3.1}$$

It can be seen from the strain-displacement equations (2.17), as well as from (2.5) and (2.9), that up to second order spatial derivatives of the horizontal and vertical displacements v and w are involved. Thus C^1 shape functions, i.e. functions with continuous derivatives, are used here. Within each element $v(s)$ and $w(s)$ are approximated by Hermitian cubics and a four point Gauss–Legendre numerical integration scheme is used.

A power law type mesh refinement near the plate's centre is adopted, namely,

$$r_n = R_A(r_o/R_A)^{\beta}, \tag{3.2}$$

where r_n is the new (refined) coordinate and r_o the old one corresponding to a uniform subdivision in $N+1$ points of the interval $[0, R_A]$. The mesh refinement exponent is denoted by $\beta(\beta > 1)$ and in all the calculations reported here $\beta = 1.25$. Some calculations were repeated with $\beta = 1.4$, while keeping the number of elements the same, but no appreciable difference in the results was observed.

An incremental Newton–Raphson algorithm based on (3.1) is adopted for the solution of the problem. However, in view of the path dependence of the constitutive equations, relatively small punch displacement increments ΔH are required. For the calculations reported here a step size $\Delta H = 0.002 R_p$ is used, the choice in this case being dictated by a $O(10^{-3})$ accuracy requirement on the strains. It should also be noted that in view of the small punch displacement increment used only one iteration per step is required for convergence.

The punch stiffness parameter, k, (see (2.19) for its definition) is taken to be $kh/E = 50$. For this value of k the penetration distance, d, (defined in (2.20)) never exceeds $10^{-4} R_p$. All the numerical calculations presented are performed by using $N = 50$ elements. A few calculations have been repeated with $N = 40$ and $N = 100$ elements but no difference in the strain predictions is observed until after the onset of localization (in which case the shell becomes unstable anyway).

Finally, the onset of localization is detected by checking the sign of the determinant (2.35) at every integration station in every element of the shell. The first time (as the punch advance H increases) that a non-positive 'stability' determinant is found, signals the onset of localization for that particular state of deformation. It should also be mentioned at this point that all the through the thickness integrals included in the computations (see (2.29) and (2.31)) are numerically evaluated using a 21-point Simpson rule.

4. Experimental procedure

The material used in the experiments, whose chemical composition is given in table 1, was cold rolled and batch annealed mild steel of two different thicknesses. The thickness of one batch was 0.056 in while the other batch was prepared by grinding down the 0.056 in material to a thickness of 0.028 in. The grain size, as determined by ASTM standard on all sample batches, was found to be 7.5–8.0 μm.

Table 1. Composition of mild steel

C	Mn	Sl	Al	Ni	Cr	V	Mo
0.071	0.298	0.033	0.054	0.011	0.019	0.001	—

The maximum possible thickness in commercially available (in adequate quantities from the same batch) sheet material at the time of experiments was 0.056 in. Furthermore, this being the maximum thickness used in most automotive applications, published experimental evidence† indicating significant thickness effects on the FLDs has been obtained using specimens of similar or smaller thicknesses. In addition, due to experimental limitations, the smallest punch radius, R_p, had to be larger than 0.984 in. Consequently the experimentally obtainable range for h/R_p was between 0.014 and 0.056.

Standard E8 (ASTM) specimens with a gauge length of 2 in and a width of 0.5 in were cut at 0°, 45°, 90° to the rolling direction from the aforementioned batches of steel and subjected to a uniaxial tension test. No significant difference

† With the onset of fracture as the failure criterion as discussed in the introduction.

in the resulting stress–strain curves for these three types of specimens was observed, thus justifying the hypothesis of the in plane plastic isotropy of the sheet adopted in §2. From the above data, the true-stress–natural-strain curve was computed (smooth line in figure 2) and subsequently fitted to the piecewise power law described by (2.38). The best fit was found to correspond to Young's modulus $E = 3.10^7$ lbf in^{-2}†, a yield stress $\sigma_y = 1.125 \times 104$ lbf in^{-2} and a hardening exponent $m = 4.0404$‡. The satisfactory agreement between the experimental results and the piecewise power law using the aforementioned parameters can also be seen in figure 2. The transverse plastic anisotropy ratio, R, (see (2.37)) was experimentally found to be $R = 1.8$, by measuring the ratio of transverse plastic strains in uniaxial tension test.

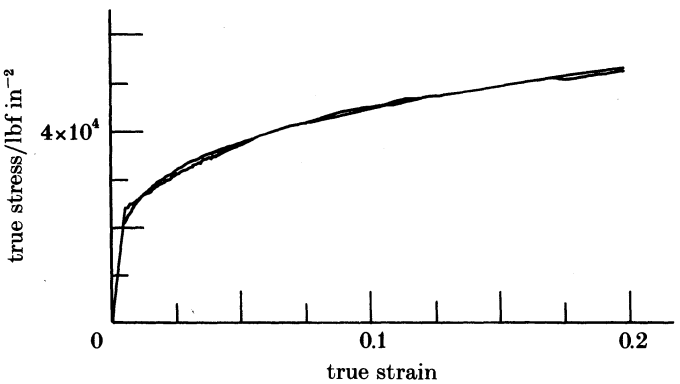

FIGURE 2. Experimentally measured and idealized uniaxial stress–strain curves for mild steel. Young's modulus, 3×10^7 lbf in^{-2}; hardening exponent, 4.0404; yield stress, 11 250 lbf in^{-2}.

The experimental determination of θ_o and θ_c, the total loading and unloading yield surface vertex angles (assuming that a vertex exists) is unfortunately not possible through direct measurements (see discussion in Hecker 1978). The choice of the aforementioned constants in this case was based on the requirement that the onset of localization for the thinnest specimen ($h = 0.028$ in, $R_p = 1.968$ in, $R_A = 2.080$ in) the computed radial strain distribution ϵ_s agrees as nearly as possible with that measured. It was thus found that the values $\theta_o = 0, \theta_c = \frac{3}{4}\pi$ gave the best fit with the experiment and have been used for all the subsequent computations.

The hemispherical punch tests were conducted by clamping the steel sheet over a lockbead and stretching the specimens by continuous punch displacement up to a desirable punch height. Three different sets of punches ($R_p = 0.984$ in, $R_p = 1.476$ in and $R_p = 1.968$ in) and three different sets of dies ($R_A = 1.050$, 1.535 and 2.080 in) have been used. A schematic diagram of the experiment is shown in figure 3*a*, plate 1 and a typical deformed specimen is depicted in figure 3*b*. An oiled 0.125 in thick polyurethane membrane was inserted between the punch and the sheet to eliminate friction between the two metal surfaces.

† 1 lbf in$^{-2} \approx 6895$ Pa.

‡ In our notation $m = 1/n$, where n is the widely used symbol for the hardening exponent in the power law $\sigma = K\epsilon^n$.

A grid made up of small circles was electrochemically etched on the top surface of the plate specimens. The engineering radial (e_1) and tangential (e_2) strain distributions on the deformed sheets were found by measuring the principal semiaxes of the resulting small ellipses. The reproducibility of the measurements was $\pm 2\%$ and the scatter of the optical measurements of e_1 and e_2 was $\pm 5\%$.

5. Results and discussion

The standard experimental practice (which was used in the construction of FLDs), for determining the limiting strains in sheet metal is by continuously deforming the sheet up to the onset of fracture (signalled experimentally by a sudden drop in load) and subsequently measuring the resulting strain distribution in the unfractured area of the shell diametrically across from the failure zone.

Although for thin sheets there is no significant difference between the strain corresponding to the onset of localized necking and the fracture strain, for thicker specimens the situation is completely different. Experimental evidence for thick sheets (see, for example, Ghosh & Hecker 1975; Hecker 1978) indicates very significant amounts of diffuse necking following the onset of localization and before fracture. The same phenomenon has been predicted theoretically in the computations of Hutchinson *et al.* (1978) where strain concentrations in the weakest cross section of the specimen have decreasing maxima and become more diffuse with increasing specimen thickness (assuming that the characteristic wavelength of the surface is kept constant). A similar type of behaviour is also exhibited by the present calculations as will be subsequently reported.

A careful measurement of the onset of necking strain is a rather involved process. In view of the construction of the punch–die arrangement, a direct measurement of the strain distribution on the sheet's surface is not possible unless the specimen is unmounted. Hence, the correct experimental determination of the onset of localization† requires the run of *many* experiments for the *same* specimen geometry with each experiment stopped at a punch height different from the previous one, in order to detect the necking. In the experiments reported here the bisection method in the interval $[0, H_f]$ with H_f the dome height corresponding to fracture has been used.

The theoretically calculated and experimentally measured strain distributions in the two extreme cases, one corresponding to the minimum amount of bending and the other corresponding to maximum bending are presented below.

Figure 4 depicts the experimentally observed and numerically calculated radial (e_1) and tangential (e_2) top surface strain distributions in a sheet of thickness $h = 0.028$ in at the onset of localization in the case of a punch with $R_p = 1.968$ in and a die with $R_A = 2.080$ in. The sheet in this case is thin ($h/R_p = 0.014$) and it behaves like a membrane as the strain distribution in figure 4 indicates.

The experiment involving the most severe bending was the one corresponding to a sheet of $h = 0.56$ in thickness using a punch with $R_p = 0.984$ in with a die

† To avoid ambiguity the experimentally observed onset of localization can be defined to occur if the maximum strain difference $(\Delta e_1)_{max}$ occurring in a zone of given width exceeds a predetermined critical number.

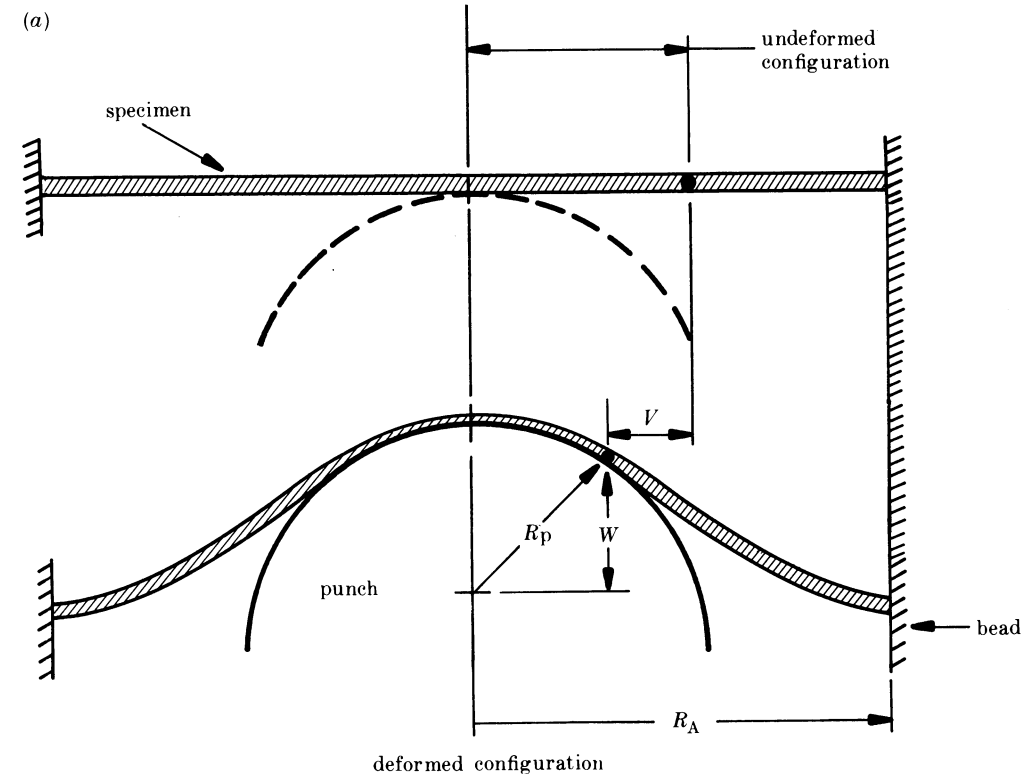

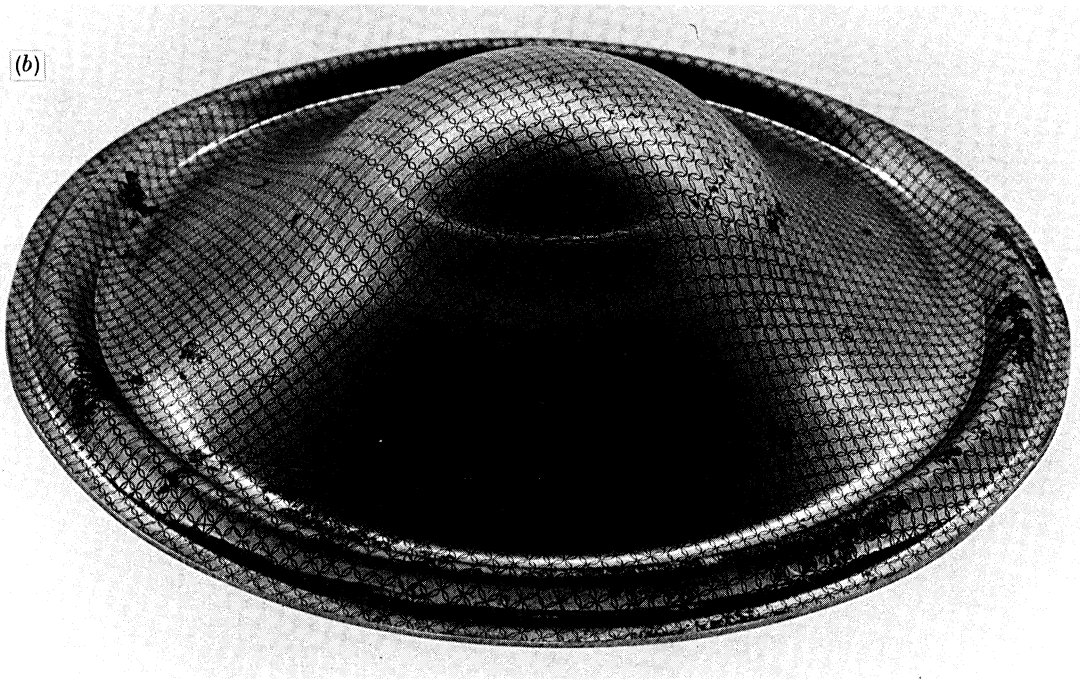

FIGURE 3. (*a*) A schematic diagram of the experiment, (*b*) a typical deformed specimen.

punch diameter/in	die diameter/in
3.937	4.160
2.953	3.073
1.968	2.100

(*Facing p.* 220)

PROCEEDINGS OF THE ROYAL SOCIETY A MATHEMATICAL, PHYSICAL & ENGINEERING SCIENCES

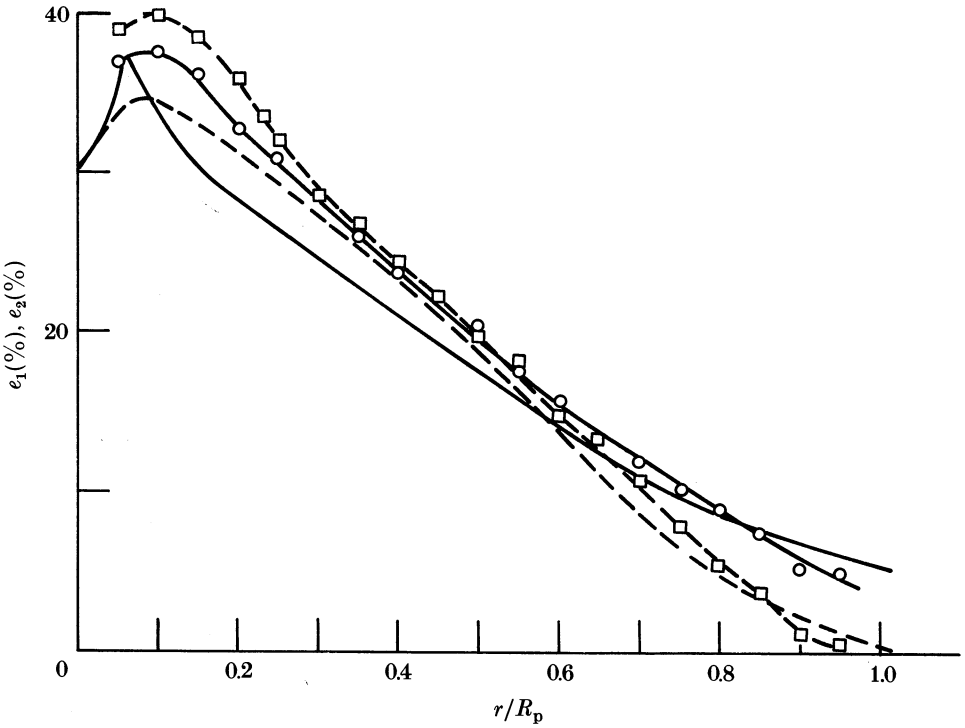

FIGURE 4. Experimentally measured and numerically calculated radial (e_1) and tangential (e_2) surface strains for the thinnest specimen ($h/R_p = 0.014$). Material, mild steel; punch to die diameter ratio, 1; sheet thickness, 0.028 in; □, e_2 experimental; – – –, e_2 theoretical; ○, e_1 experimental; ——, e_1 theoretical.

having $R_A = 2.080$ in. Figure 5 depicts the experimentally observed and numerically calculated radial (e_1) top surface strain distribution of the onset of localization. Notice the severe amount of bending present in this case ($h/R_p = 0.056$) as suggested by the sudden drop of the strain curve near the point of loss of contact between the sheet and the punch.

In order to compare the necking strains with the onset of fracture strains (which, as explained in the introduction, are the standard strains for the experimental determination of FLDs) all specimens have also been deformed up to fracture and the corresponding results are reported in table 2.

As can be seen from table 2, within the experimentally investigated ratio of thickness to punch radius h/R_p (from 0.014–0.056), the thickness increases, although it significantly alters the fracture strain and shows little effect on the localization strain as can be seen from comparison of the two extreme cases depicted in figure 4 (minimum amount of bending) and figure 5 (maximum amount of bending). To complete the investigation of the influence of bending on the localization strain numerical calculations were carried out for sheets with the same geometric and material properties but various different thicknesses up to a h/R_p ratio of 0.2.

More specifically, figure 6 investigates the effect of the experimental-arrangement

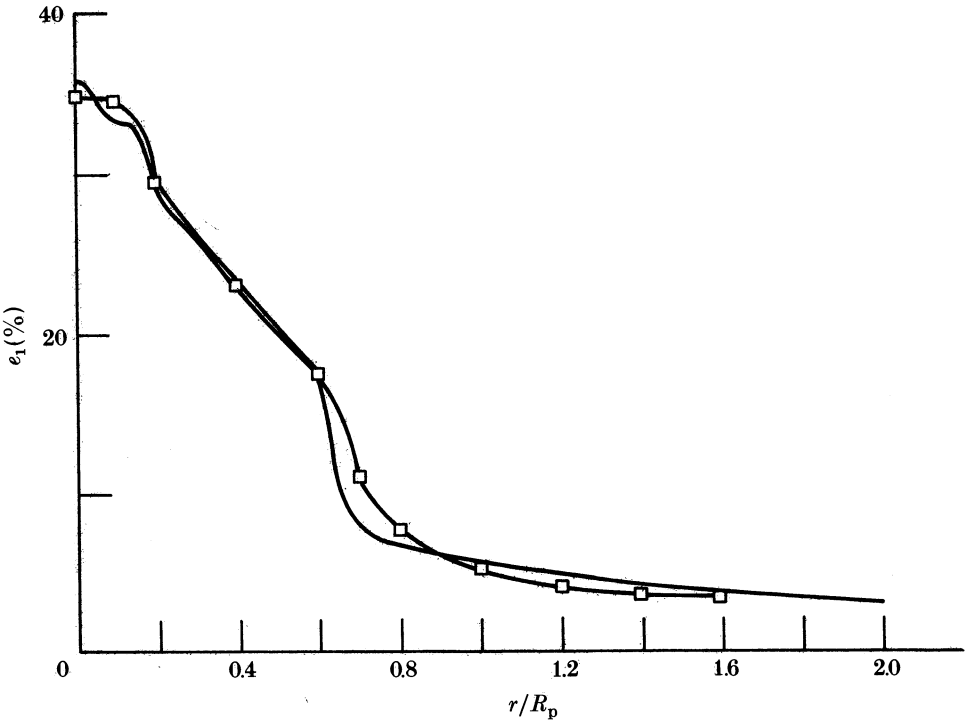

FIGURE 5. Experimentally measured and numerically calculated radial surface strains (e_1) for the thickest specimen ($h/R_p = 0.056$). Material, mild steel; sheet thickness, 0.056 in; punch to die diameter ratio, 0.5; □, e_1 experimental; ——, e_1 theoretical.

TABLE 2. COMPARISON OF NECKING AND FRACTURE STRAINS FOR DIFFERENT SPECIMENS

		thickness (h)			
		0.028 in		0.056 in	
(R_p) punch radius/in	(R_A) die aperture radius/in	necking (%)	fracture (%)	necking (%)	fracture (%)
1.97	2.08	36	41	36	66
1.48	2.08	34	39	34	61
	1.54	34	41	36	53
0.98	2.08	35	42	36	62
	1.54	35	44	36	64
	1.05	36	45	36	67

geometry (R_A/R_p ratio) on the curve of critical radial top surface strain $(e_1)^s_{cr}$† against thickness (h/R_p).

As expected, the critical strain increases with increasing thickness from about 0.35 for $h/R_p = 0.05$ to about 0.45 for $h/R_p = 0.2$ but does not seem to be significantly affected by the geometry.

† Only the e_1 against h/R_p curves are depicted here since in view of the frictionless condition $e_1 \approx e_2$ in the failure zone.

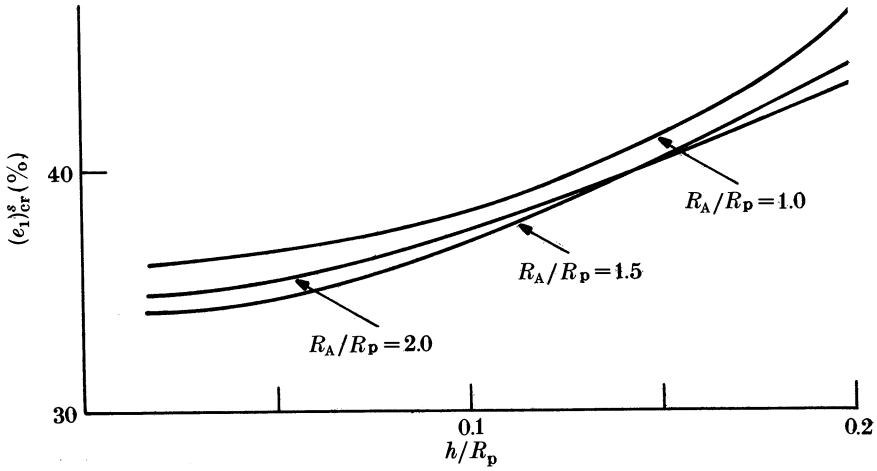

FIGURE 6. Effect of geometry on the critical strain against thickness curve. $\nu = 0.30$, $\epsilon_y = 3.75 \times 10^{-4}$, $m = 4.0404$, $\theta_0 = 0$, $\theta_c = \frac{3}{4}\pi$, $R = 1.8$.

All the above reported computations have been performed for a constitutive model having vertex angles $\theta_o = 0$, $\theta = 3\pi/4$ which were chosen in order to give a 'best fit' of the strain distribution at necking with the experimental results in the case of the 'thinnest' sheet ($h/R_p = 0.014$), as previously explained. To complete this investigation the effect was studied of the change of the vertex characteristics of the model (keeping all other directly measurable material properties such as E, σ_y, m, R, fixed) on the critical top surface strain $(e_1)^s_{cr}$ to thickness h/R_p) curve. Figure 7 depicts the results of these calculations (in the case

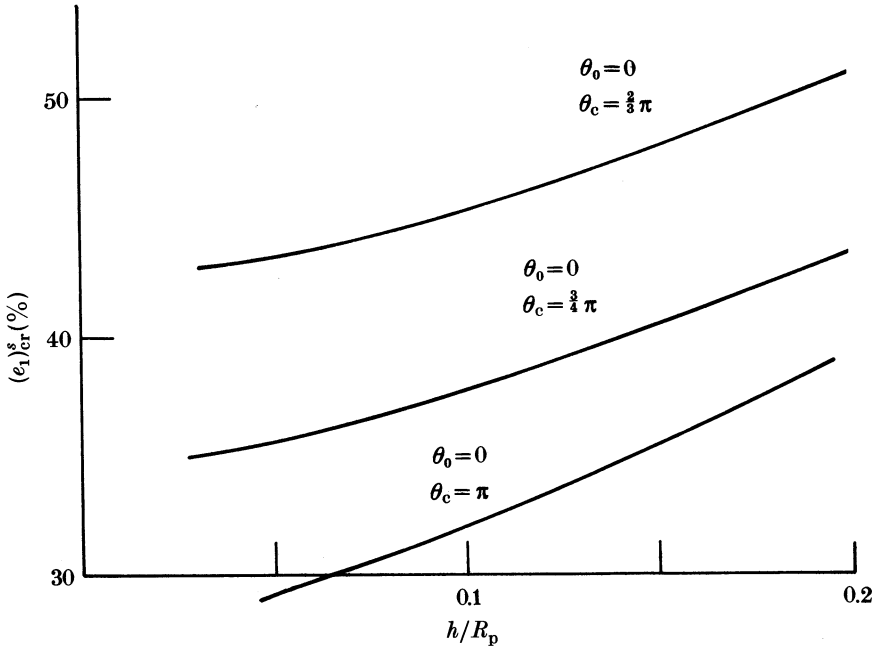

FIGURE 7. Effect of material's vertex characteristics on the critical strain against thickness curve. $\nu = 0.30$, $\epsilon_y = 3.75 \times 10^{-4}$, $m = 4.0404$, $R = 1.8$, $R_A/R_p = 1.0$.

of $R_A/R_p = 1$) for three different cases: the stiffest, $\theta_o = 0$, $\theta_c = \frac{2}{3}\pi$; $\theta_o = 0$, $\theta_c = \frac{3}{4}\pi$, and the least stiff $\theta_o = 0$, $\theta_c = \pi$. Notice that as the lower critical strains correspond to the less stiff material. The results in this case indicate roughly the same increase in critical strain for the same increase in sheet thickness regardless of the details of the vertex characteristics of the material (observe that the three curves appear to be almost parallel).

Two remarks may be made here about the finite element calculations. For thin sheets it was observed that after the onset of localization a small increase in punch height (of about $\frac{1}{10}\,h$ or less) produced large increases in the strains of the element containing the cross section at which localization first occurred. For greater thicknesses, the same increase in punch height produced considerably smaller strain increases distributed over a larger number of elements near the 'critical' one thus indicating the presence of a more diffuse type of necking for the thicker sheets. It was also noticed that for thinner sheets, the strain quantity that had the greatest increases after the onset of localization was the mid-surface radial strain ϵ_s while for thicker ones the strain quantity that was growing more rapidly than the others was the curvature strain $\hat{k}_s$.

The other remark pertains to the location of the necking zone, which was numerically found to recede progressively from the apex as the thickness increased, a fact that has also been observed experimentally.

6. Conclusions

The purpose of this investigation is to provide some theoretical insight into the hitherto little explored area of thickness effects on the necking of biaxially stretched metallic sheets.

An appropriate nonlinear shell theory capable of incorporating large rotation as well as large strain effects has to be introduced for the analysis of this problem in view of the inadequacy of the membrane approach which is routinely employed in similar calculations (involving large deformations of sheet metal). Consistently with the proposed shell theory a novel, closed form, localization criterion is developed for prediction of the localization instability in the shell.

A very good correlation is found between the numerically calculated (using an FEM approach based on the shell theory described here) and experimentally measured surface strain distributions in circular plates deforming over rigid hemispherical punches. In addition the calculations do predict the experimentally observed phenomenon of more diffused necking and lower strain peaks, following the onset of localization, with increasing plate thickness.

The distinction between the onset of necking and the onset of fracture although unimportant for thin sheets becomes increasingly important for thicker ones in view of the progressively larger amount of post-localization necking as the thickness increases before fracture. In contrast to similar works in the literature, careful experimental distinction of these two phenomena is made in this investigation.

By using the onset of necking as the failure criterion in this work it was found from experiments as well as from analytical modelling, that the thickness:

(punch) radius of curvature ratio does not have any important effects on the critical strain until this ratio starts exceeding 0.10–0.15, i.e. until the sheet becomes considerably thick. This relative insensitivity of the critical strain on the thickness for the thinner sheets is attributed to the rather low hardening of the material investigated which in turn implies (for given bending strain) that the middle surface stretching strain is much more important than the bending one.

The only results obtained in this work are near the balanced biaxial stretching region ($\rho^* = 1$) of the FLD. The insensitivity of the result to the details of the punch geometry (for given thickness to radius of curvature ratio) is a logical consequence (almost proportional loading near the critical area of the shell).

Support for this work by the National Science Foundation (NSF MEA 8116449) and Ford Motor Company is gratefully acknowledged. The authors also thank Mr J. R. Bales and Mr G. Grab for their help in the experimental part of this investigation and Mr H. Schyten and Mr W. Lee for their help in running the FE code.

Appendix

The incremental compliance tensor relating $\boldsymbol{E}$ to $\overset{\nabla}{\boldsymbol{t}}$ is given by

$$\partial^2 W/\partial \overset{\nabla}{T}{}^{ij}\,\partial \overset{\nabla}{T}{}^{kl} = M_{ijkl} + f(\theta)\,[(1-k(\theta)\cot\theta)\,C_{ijkl} + k(\theta)\cot\theta(p_{ij}\,p_{kl}+q_{ij}\,q_{kl}) - k(\theta)\,(p_{ij}\,q_{kl}+p_{kl}\,q_{ij})] + \tfrac{1}{2}f''(\theta)\,q_{ij}\,q_{kl}, \quad \text{(A 1)}$$

where the elastic compliances M_{ijkl} are given by (2.42), the plastic ones C_{ijkl} by (2.36) and where $k(\theta) = -f'(\theta)/2f(\theta)$. Also

$$p_{ij} = \left[\left(\frac{1}{E_s}-\frac{1}{E}\right)\frac{\partial^2\phi}{\partial\tau^{ij}\,\partial\tau^{kl}}\overset{\nabla}{T}{}_{kl} + \left(\frac{1}{E_t}-\frac{1}{E_s}\right)\frac{\dot\tau_e}{\tau_e}\frac{\partial\phi}{\partial\tau^{ij}}\right]\cos\theta \div \left[\dot\tau_e\left(\frac{1}{E_t}-\frac{1}{E}\right)^{\frac{1}{2}}\right] \quad \text{(A 2)}$$

$$q_{ij} = \left\{\cos^2\theta\left[\left(\frac{1}{E_s}-\frac{1}{E}\right)\frac{\partial^2\phi}{\partial\tau^{ij}\,\partial\tau^{kl}}\overset{\nabla}{T}{}^{kl}\right] + \left[\cos^2\theta\left(\frac{1}{E_t}-\frac{1}{E_s}\right)-\left(\frac{1}{E_t}-\frac{1}{E}\right)\right]\frac{\dot\tau_e}{\tau_e}\frac{\partial\phi}{\partial\tau^{ij}}\right\} \div \left\{\sin\theta\left[\dot\tau_e\left(\frac{1}{E_t}-\frac{1}{E}\right)^{\frac{1}{2}}\right]\right\}. \quad \text{(A 3)}$$

The unloading vertex angle, θ_c, is defined to be the angle between the cone axis, λ, and the tangent, $\boldsymbol{\tau}^*-\boldsymbol{\tau}$, from point $\boldsymbol{\tau}$ to the initial yield surface in the stress space; $\boldsymbol{\tau}^*$ is the position vector of the corresponding point of contact on the initial yield surface. According to the above definitions

$$\cos\theta_c = [(\tau^{*ij}-\tau^{ij})\,C_{ijkl}\,\lambda^{kl}]/[(\tau^{*ij}-\tau^{ij})\,C_{ijkl}(\tau^{*ij}-\tau^{kl})]^{\frac{1}{2}}. \quad \text{(A 4)}$$

The normality condition between $\partial\phi/\partial\boldsymbol{\tau}^*$ and $\boldsymbol{\tau}-\boldsymbol{\tau}^*$, is

$$\partial\phi/\partial\tau^{*ij}(\tau^{ij}-\tau^{*ij}) = 0 \quad \text{(A 5)}$$

and the fact that τ^{*ij} lies on the initial yield surface gives

$$\tau^{*ij}\,\partial\phi/\partial\tau^{*ij} = \sigma_y^2. \quad \text{(A 6)}$$

By substituting from (A 5) and (A 6) into (A 4) and by using also (2.36), one finally has for θ_c

$$\tan\theta_c = -\frac{\sigma_y}{(\tau_e^2-\sigma_y^2)^{\frac{1}{2}}}\left(\frac{E_s^{-1}-E^{-1}}{E_t^{-1}-E^{-1}}\right)^{\frac{1}{2}} \tag{A 7}$$

which coincides with the expression obtained by Christoffersen & Hutchinson (1979) for the case of the Von Mises initial yield surface.

References

Asaro, R. & Needleman, A. 1984 *Scr. metall.* **18**, 429–435.

Asaro, R. & Needleman, A. 1985 *Acta metall.* **23**, 923–953.

Budiansky, B. 1959 *J. appl. Mech.* **26**, 259–264.

Christoffersen, J. & Hutchinson, J. W. 1979 *J. Mech. Phys. Solids* **27**, 465–487.

Ghosh, A. K. & Hecker, S. S. 1975 *Metall. Trans.* **6A**, 1065–1074.

Goetz, A. 1970 *An introduction to differential geometry*. Reading, Massachusetts: Addison-Wesley.

Hecker, S. S. 1976 *Constitutive equations in viscoplasticity, computational and engineering aspects, A.M.D.*, vol. 20, pp. 1–33. New York: ASME.

Hecker, S. S. 1978 *Applications of numerical methods to forming processes, A.M.D.*, vol. 28, pp. 85–94. New York: ASME.

Hiam, J. R. & Lee, A. P. 1978 *Sh. Metal Inds* **55**, 631–641.

Hill, R. 1952 *J. Mech. Phys. Solids* **1**, 19–30.

Hill, R. 1967 *J. Mech. Phys. Solids* **15**, 79–95.

Hutchinson, J. W. 1970 *Proc. R. Soc. Lond.* A **319**, 247–272.

Hutchinson, J. W. 1974 *Advances in applied mechanics*, vol. 14, pp. 67–144. New York: Academic Press.

Hutchinson, J. W., Neale, K. W. & Needleman, A. 1978 *Mechanics of sheet metal forming*, pp. 111–126. New York: Plenum Press.

Keeler, S. P. & Backofen, W. A. 1963 *Trans. Am. Soc. Metals* **56**, 25–48.

Krauss, H. 1967 *Thin elastic shells*. New York: John Wiley.

Kula, E. B. & Fahen, N. H. 1961 *Mater. Res. Stand.* **1**, 631–636.

Lin, T. H. 1971 *Advances in applied mechanics*, vol. 11, pp. 255–311. New York: Academic Press.

Marciniak, Z. & Kuczynski, K. 1967 *Int. J. mech. Sci.* **9**, 609–620.

Needleman, A. & Triantafyllidis, N. 1978 *J. engng Mater. Technol.* **100**, 164–169.

Oden, J. T. & Kikuchi, N. 1984 *Finite elements: special problems in solid mechanics* (ed. J. T. Oden and G. F. Carey), vol. 5, pp. 158–212. New Jersey: Prentice Hall.

Stören, S. & Rice, J. R. 1975 *J. Mech. Phys. Solids* **23**, 421–441.

Triantafyllidis, N. 1985*a* *J. Mech. Phys. Solids* **33**, 117–139.

Triantafyllidis, N. 1985*b* *Plastic instability: Proceedings of the international symposium on plastic instability*, pp. 115–124. Paris: Presses de l'Ecole Nationale des Points et chaussees.

Wang, N. M. & Budiansky, B. 1978 *J. appl. mech.* **45**, 73–82.

PROCEEDINGS OF THE ROYAL SOCIETY A MATHEMATICAL, PHYSICAL & ENGINEERING SCIENCES

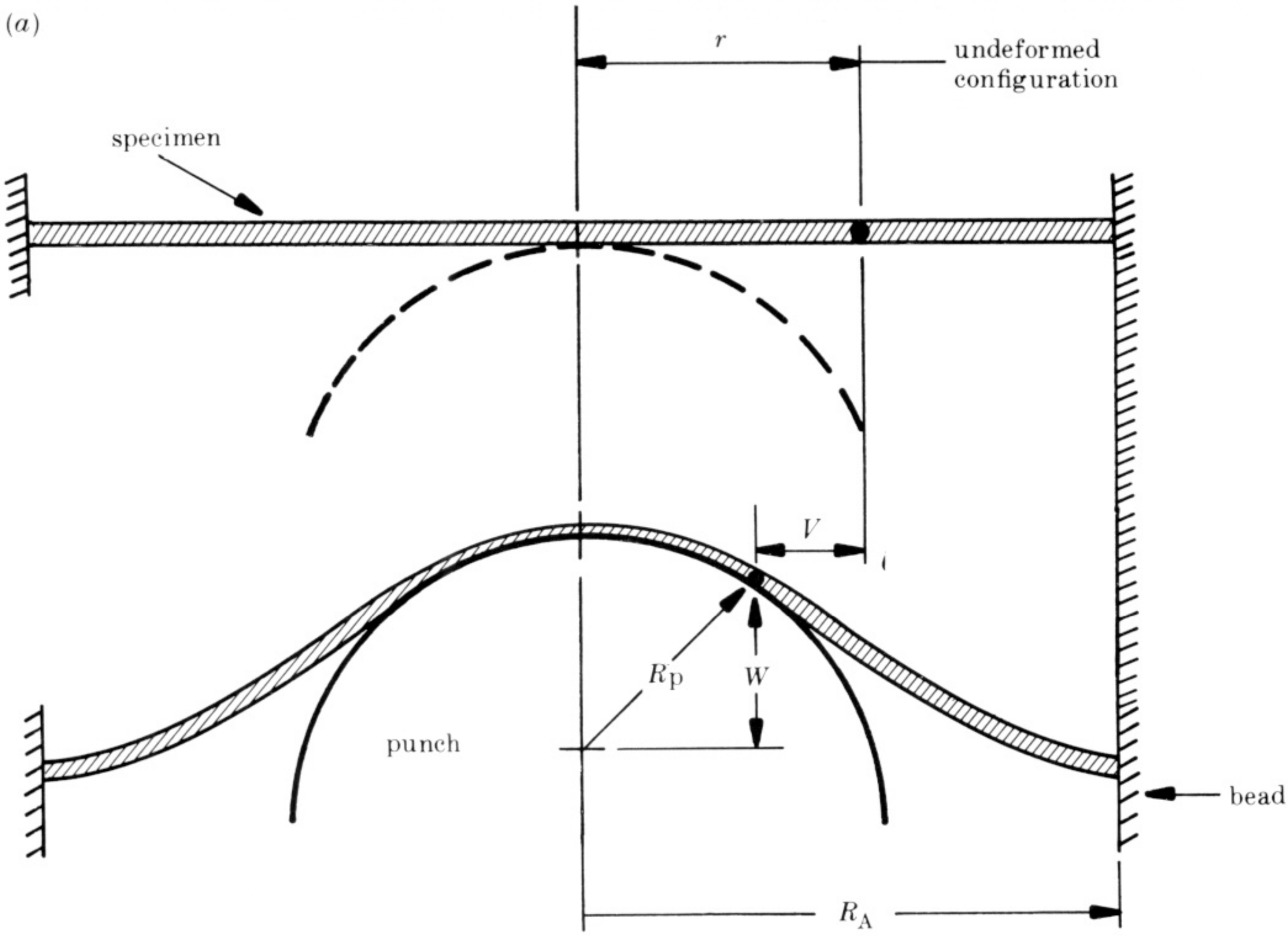

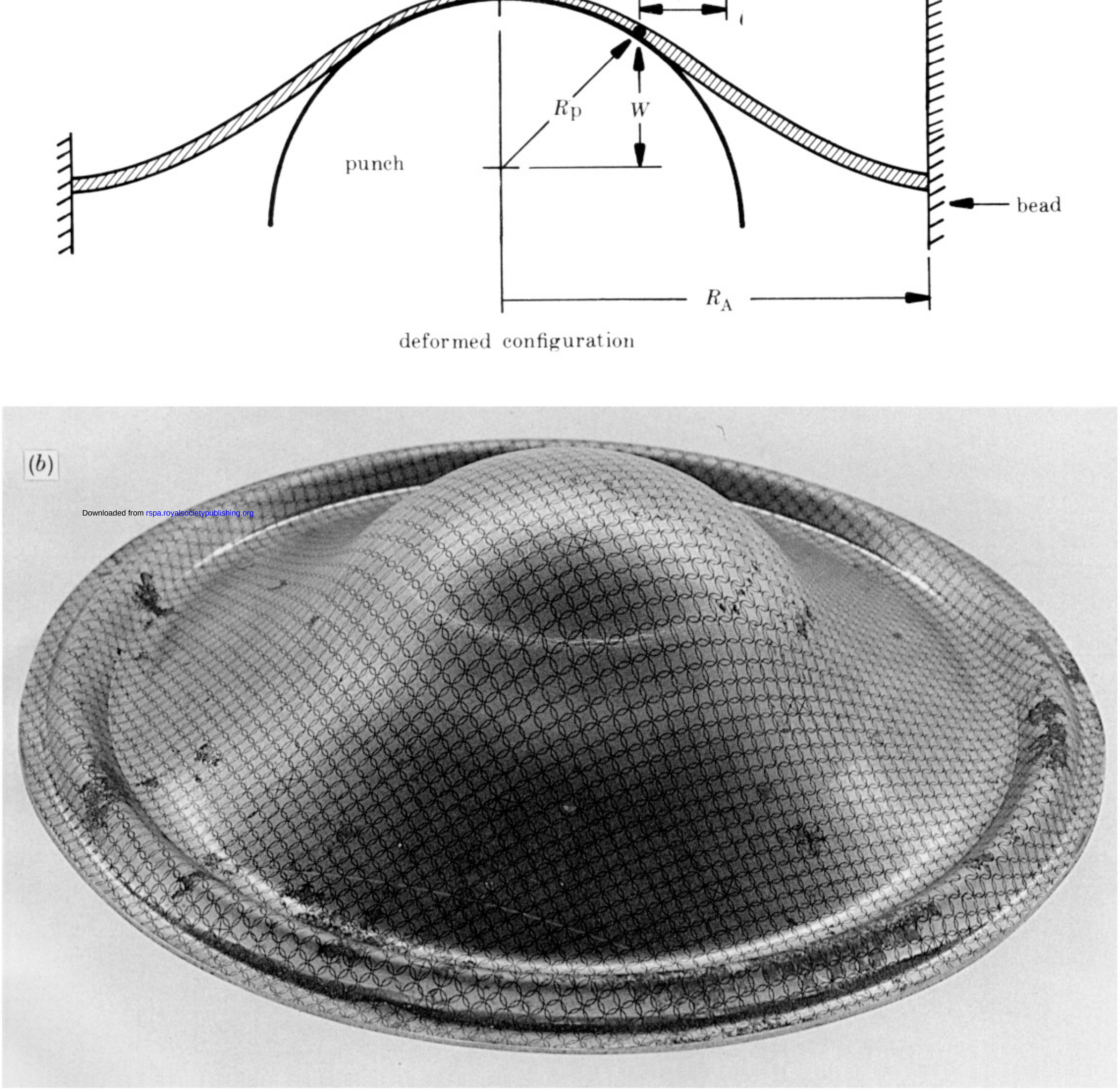

PROCEEDINGS OF THE ROYAL SOCIETY A MATHEMATICAL, PHYSICAL & ENGINEERING SCIENCES

FIGURE 3. (*a*) A schematic diagram of the experiment, (*b*) a typical deformed specimen.